Food & Function

ROYAL SOCIETY OF CHEMISTRY

PAPER

View Article Online
View Journal | View Issue

Check for updates

Cite this: *Food Funct.*, 2022, **13**, 7123

Building blocks of β-sitosterol-γ-oryzanol gels revealed by small-angle neutron scattering and real space modelling†

Elliot Paul Gilbert [a,b]

Mixtures of β-sitosterol and γ-oryzanol form gels in a range of organic solvents. Despite being widely studied, particularly as potential oleogels for food application, details of the intrinsic gel-forming building blocks remain unclear. Small-angle neutron scattering (SANS) combined with solvent contrast variation has been used to evaluate potential structural models. While evidence exists that the building blocks are hollow cylinders (tubules), the simultaneous fitting of twelve contrast-varied SANS data sets indicates that the previously proposed model of double walled tubules is incorrect. Predicted scattering based on real space models provides compelling evidence that the origin of the gelling behaviour is the limited assembly of adjacent tubules to form a space-filling network of fibrils.

Received 7th April 2022,
Accepted 1st June 2022

DOI: 10.1039/d2fo00935h

rsc.li/food-function

Open Access Article. Published on 02 June 2022. Downloaded on 12/6/2025 6:49:25 AM.
This article is licensed under a Creative Commons Attribution 3.0 Unported Licence.

Introduction

The structure of oil-continuous products, such as margarine or butter, is based on a three-dimensional network of small crystallites of triglycerides (also known as triacylglycerols or TAGs). However, there is motivation to replace such lipids, that are rich in saturated fatty acids and whose consumption is known to raise serum low-density lipoprotein cholesterol levels, with monounsaturated and polyunsaturated fatty acids to assist in reducing the risk of cardiovascular disease. Any radical alternative to TAGs in structuring oils would need to decouple providing firmness to a product from raising blood cholesterol levels.[1] Plant-based oils, rich in unsaturated fatty acids, do not provide an appropriate macroscopic structure that is essential for many food products due to their being liquid at ambient temperature. Partial hydrogenation of unsaturated fats has been one approach explored; however this yields trans fats that have the dual negative effects of both raising low-density lipoprotein while simultaneously lowering high-density lipoprotein. Consequently, driven by consumer demand, as well as government regulation, there has been a major emphasis within the food industry to find alternative methods to replace such trans and saturated fats with "healthier" alternatives while[2] simultaneously maintaining consumer perception and acceptance.

One such approach is oleogelation where non-TAG-based gelator molecules can be incorporated into liquid oils to form gels. Oleogelation can be achieved using natural waxes, phospholipids including lecithin, mono- and di-glycerides, fatty alcohols and fatty acids, proteins and functionalised polysaccharides, with the molecules arranging themselves into a 3D network that can entrap oil. Such oleogels could then be used to form the oil phase of O/W or W/O emulsions. One of the most studied oleogel systems is γ-oryzanol (a sterol ester) mixed with a variety of phytosterols. The consumption of phytosterols reduces blood cholesterol which is commonly accepted to occur due to competition between cholesterol and phytosterols for incorporation into intestinal mixed micelles as well as poor intestinal absorption of phytosterols. This reduced uptake of cholesterol does not lead to a matching increase in cholesterol synthesis but rather to an overall decrease in blood cholesterol levels and an effective increase in fecal excretion.[3] Oleogel systems based on phytosterols therefore have the potential dual benefit of directly reducing cholesterol as well as providing an approach to reducing the need for saturated fats for structuring products.

While oleogels are understandably characterised by rheological studies and texture, an understanding of the structural basis for gel formation is critical. Information can, in principle, be obtained from optical microscopy but this is challenging if the system is transparent as is the case for γ-oryzanol – phytosterol gels. Electron microscopies (SEM and TEM) are possible but also problematic; they are affected by the limited contrast between the gelator molecules with respect to the

[a]*Australian Centre for Neutron Scattering, Australian Nuclear Science and Technology Organisation, Locked Bag 2001, Kirrawee DC, NSW 2232, Australia. E-mail: elliot.gilbert@ansto.gov.au*
[b]*Australian Institute for Bioengineering and Nanotechnology and Centre for Nutrition and Food Sciences, The University of Queensland, St Lucia, Brisbane, QLD 4072, Australia*

† Electronic supplementary information (ESI) available. See DOI: https://doi.org/10.1039/d2fo00935h

Open Access Article. Published on 02 June 2022. Downloaded on 12/6/2025 6:49:25 AM.
This article is licensed under a Creative Commons Attribution 3.0 Unported Licence.

organic solvent, require exposure of the sample to vacuum leading to oil loss, and intense electron beams, both leading to potential structural artefacts. As a complementary approach, small-angle scattering methods have a number of unique advantages. The spatial dimensions from small-angle X-ray (SAXS) and neutron scattering (SANS) extend from the sub-nanometre to hundreds of nanometre range; this makes them particularly attractive to enable structural relationships to be established between the gelling behaviour and the underlying structures necessary for gel formation to occur. There are also no special sample preparation requirements; the samples can be presented to the beam at atmospheric pressure, and without staining, enabling materials to be studied in their 'native' state. Opportunities in the application of SAXS and SANS to food materials and oleogels can be found elsewhere.[4–6]

SAXS has shown that mixtures of β-sitosterol with γ-oryzanol self-assemble in triglyceride oil to form hollow cylindrical structures, referred to as tubules.[7–21] Similar structures are observed when sitosterol is replaced with ergosterol, stigmasterol, cholesterol and cholestanol. The tubule diameter in the γ-oryzanol – phytosterol system varies between 67 and 80 Å with a greater number of sterol double bonds resulting in a narrowing of the tubule diameter.[7] Wall thicknesses have been estimated to be 8–12 Å depending on phytosterol;[11] the latter was claimed to be comparable in size to the length of the long axis of the characteristic rigid four-ring system for sterol molecules, suggesting that the flexible acid and alkyl moieties do not leave a characteristic signature in the SAXS (Fig. S1†). Due to the additional molecular group in the sterol ester with respect to the sterol (Fig. S1†), the intermolecular packing may predispose the tubules to take the form of helical ribbons, reminiscent of structures reported earlier in steroid systems.[22–24] Importantly the tubules formed have structures that are unrelated to the structures of the individual gelator molecules;[7] indeed, the individual molecules are unable to form gels by themselves indicating some degree of cooperativity with γ-oryzanol exhibiting a far greater affinity for oil than β-sitosterol.[7] Infra-red spectroscopy indicates that the two molecules interact through intermolecular hydrogen bonding with optimal gelling occurring at equimolar ratio.[7]

When these oleogels form the oil phase of W/O and O/W emulsions, larger dimension fibres are formed; this differs from the self-assembled tubules detected in the oleogels that are too thin to be observed by light microscopy. In addition, SAXS shows the presence of β-sitosterol monohydrate crystals which form in emulsions with a relatively polar organic phase (dielectric constant >2.5) and, for W/O emulsions, a high water activity of greater than 0.9 which can be modulated by the presence of NaCl.[15] The associated scattering patterns from these emulsions are reminiscent of those for the oleogels in pure triglyceride oil, except that the first broad peak in the scattering pattern develops into a distorted or asymmetric, possibly double, peak. The distorted peak does not allow fitting of the data to a hollow tube model used for the pure oleogels but the data can be simulated (qualitatively) using a combination of two hollow tubes of 70 and 100 Å diameter. The physical interpretation for such behaviour was not obvious; it could either indicate that the structure of the wall is more complicated than in the pure oleogel or the system comprises two different types of tubules, where the second type is formed under the influence of the presence of water. Non-uniaxial extended structures, *e.g.* parallelepipeds or hollow cylinders with elliptical cross-section, could also be envisaged.[25] In more recent work, it was noted that the use of oils with low dielectric constant (*i.e.* non-edible long chain hydrocarbons such as decane) in the oil phase decreases the availability of water molecules in the oil phase substantially, thereby eliminating the formation of monohydrate sterol crystals. Thus, in the absence of water, and when formed in decane, no such double peak formation would be anticipated. However. despite this, peak distortion has been observed to occur in oleogels themselves, the extent of which is influenced by solvent polarity although this was not discussed in detail.[15] Oil polarity may also affect tubule persistence length; SEM studies of tubules in decane are observed to be curly whereas, with increasing dielectric constant of the oils (*e.g.* sunflower oil), the tubules become elongated;[18] irrespective, tubule lengths of several micrometers are commonplace.

As a means to better understand the structure of the building blocks, SANS provides complementary structural information to small-angle X-ray scattering (SAXS) but has the advantage that scattering contrast can be manipulated by varying deuterium content. While this is typically achieved in aqueous systems by mixing H_2O and D_2O, it is also possible in lipophilic systems.[26,27] Bot *et al.* employed SANS from both oleogel (organogel in the case of non-edible oils) and associated emulsion systems in which the solvent comprised mixtures of sunflower oil and either non-deuterated (*i.e.* normal) or deuterated decane.[12] From their SANS data, they proposed a more complex double-walled tubule structure. As such, while the inner wall had been observed in SAXS before, the origin of the outer wall was less clear but speculated to be associated with ferulic acid moieties from γ-oryzanol sticking out of the tubules. The latter become observable due to differences in neutron scattering length density (SLD) between the molecular regions which are not amenable to SAXS (Table 1). However, within the constraints of the data available, the structure elucidation was limited to only a semi-quantitative assessment. Here, SANS has been applied to investigate what was anticipated to be a 'simpler' system in which gels have been prepared in mixtures of decane and its deuterated analogue so that variations in contrast with respect to the sitosterol – oryzanol structurant could be explored without changing the physical properties, *i.e.* polarity, of the organic phase. However, as will be shown, the system remains complex. Global refinement of the SANS data indicates that the scattering is inconsistent with a double walled tubule structure; however, in combination with real space modelling details of the gel building blocks are revealed.

 This journal is © The Royal Society of Chemistry 2022

Open Access Article. Published on 02 June 2022. Downloaded on 12/6/2025 6:49:25 AM.
This article is licensed under a Creative Commons Attribution 3.0 Unported Licence.

Table 1 Chemical formulae, neutron and X-ray scattering length densities for the components used for preparing oleogels

	Formula	X-ray SLD/ 10^{-6} Å^{-2}	Neutron SLD/ 10^{-6} Å^{-2}	Neutron contrast match (C10D volume fraction)
β-Sitosterol	$C_{29}H_{50}O$	9.52	0.168	0.0928
γ-Oryzanol	$C_{40}H_{58}O_4$	9.32	0.721	0.171
Androsterol	$C_{19}H_{30}O$	9.43	0.437	0.131
Ferulic acid (minus O)	$C_{10}H_9O_3$	8.94	1.71	0.311
Alkyl (1-decene)	$C_{10}H_{20}$	7.15	−0.265	0.0316
Decane (non-deuterated)	$C_{10}H_{22}$	7.15	−0.488	—
Decane (deuterated)	$C_{10}D_{22}$	7.15	6.58	—

Neither sitosterol nor oryzanol are pure components. γ-oryzanol data are based on oryzanol A (cycoartenyl ferulate); the alkyl formula is based on the molecular structure of oryzanol A minus its sterane core (androsterol). Ferulic acid has the formula $C_{10}H_{10}O_4$. Molecular structures for the gelators are shown in Fig. S1.†

Experimental

γ-Oryzanol (Tsuno Rice Fine Chemicals, Wakayama, Japan) and tall oil sterol (78.5% β-sitosterol, 10.3% β-sitostanol, 8.7% campesterol and 2.5% of other minor sterols, Unilever, the Netherlands) were used as structurants. These molecules are shown in Fig. S1.† Each sample contained 32% w/w of the gelator mixture, namely β-sitosterol – γ-oryzanol, at 40 : 60 relative weight per cent (corresponding to an equimolar ratio) in the organic phase comprising mixtures of *n*-decane (>99%, Sigma-Aldrich, The Netherlands) and deuterated *n*-decane (D-enrichment > 98.5%, Acros Organics). Twelve solvents differing by the relative mass percentage of decane and deuterated decane were prepared to enable the manipulation of contrast in neutron SLD for subsequent SANS experiments: 0 (*i.e.* decane, denoted C10H), 7.3, 14.6, 20.0, 24.2, 30.3, 34.7, 39.0, 54.1, 69.8, 83.8 and 100 (*i.e.* deuterated decane, denoted C10D); by volume per cent these are 0, 6.4, 12.9, 17.8, 21.7, 27.3, 31.5, 35.6, 50.4, 66.7, 81.8 and 100. The gel samples were subsequently prepared by dissolving the structurants in the solvents at elevated temperature (100 °C). Chemical formulae, physical densities and neutron and X-ray SLDs for the components used for preparing oleogels are summarised in Table 1.

SANS experiments were performed on the QUOKKA SANS instrument at ANSTO.[28] The gels were placed in demountable cells with quartz windows and with 1 mm sample path length. Solvents were placed in a Hellma quartz cuvette of the same thickness. Three configurations were used to cover a q range of 0.004–0.7 Å^{-1} where q is the magnitude of the scattering vector = $(4\pi/\lambda)\sin(\theta)$, λ is the wavelength and 2θ is the scattering angle. These configurations were: (i) source-to-sample distance (SSD) = 20.3 m, sample-to-detector distance (SDD) = 20.1 m, (ii) SSD = 3.96, SDD = 4.04 m, (iii) SSD = 12.0 m, SDD = 1.35 m using a λ of 5 Å with 10% resolution. Source aperture and sample aperture diameters were 50 mm and 10 mm respectively. A temperature-controlled 20 position sample changer was used operating at 25 °C. Additional measurements were performed at 18, 35, 45 and 55 °C but showed little change compared to 25 °C data and are therefore not discussed here.

Data were reduced using the NIST NCNR SANS reduction macros[29] modified for QUOKKA, using the Igor software package (Wavemetrics, Lake Oswego, OR) with data corrected for empty cell scattering, transmission and detector sensitivity. Data were transformed onto an absolute scale using attenuated direct beam transmission measurements. Subsequent reduction involved subtraction of the corresponding solvent scattering from the oleogel scattering based on the total solvent volume fraction. Specifically, 32% w/w in decane is equivalent to 25.6 volume% and 28.4 volume% in the more dense solvent; SANS data thus required the subtraction of 74.4% and 71.6% of the corresponding solvent scattering signal respectively from the total gel scattering. Complementary SAXS measurements were performed on a Bruker Nanostar instrument as described previously[30] on the non-deuterated sample. Due to the gel nature of the sample, it was not possible to fill a standard narrow bore quartz capillary for the SAXS measurements; instead, a quantity of the sample, of unknown thickness, was located between two sheets of 3M™ tape.

Reciprocal space models were generated and developed in Igor (Wavemetrics) by the author[12] with some fitting also conducted in SASView.[31] The generation of theoretical scattering functions from real space structures was carried out using the Real Space modelling module of the NCNR SANS macros[29] written for Igor and cross-referenced against Singlebody[32] and McSIM.[33]

Results and discussion

The SANS from the β-sitosterol : γ-oryzanol gels for the twelve contrasts investigated is shown in Fig. 1 following removal of empty cell background scattering; all data are on an absolute scale while still containing the corresponding solvent scattering. The scattering comprises decreasing intensity at low q, followed by a series of broad oscillations with the observable number depending on contrast. For 100% C10D, the oscillations are located at ≈0.1, 0.19, 0.29 and 0.37 Å^{-1}. In previous SAXS studies, such scattering was attributed to hollow cylindrical structures, described as tubules, with finite wall thickness. Such oscillations are rarely observed in scattering measurements, typically being smeared out by a finite size distribution

Open Access Article. Published on 02 June 2022. Downloaded on 12/6/2025 6:49:25 AM.
This article is licensed under a Creative Commons Attribution 3.0 Unported Licence.

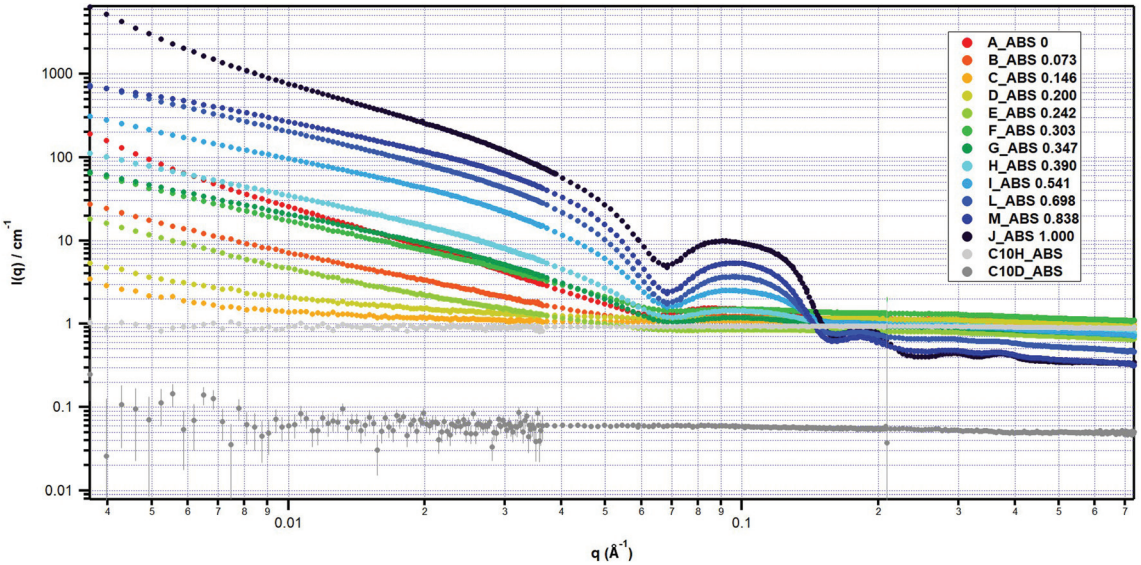

Fig. 1 SANS from solvent contrast variation series of gels. Sample cuvette scattering has been removed but data are prior to solvent-background subtraction. The values in the legend correspond to the mass fraction of C10D in the C10H : C10D solvent mixture.

of the scattering objects; their presence here is evidence of a high degree of monodispersity *i.e.* narrow size distribution. For a solid cylinder, at q values $\gg L^{-1}$ (where L is the length of the cylinder), the scattering decays as q^{-1} until $q \gg R^{-1}$ where it decays as q^{-4} (Porod scattering) although the latter is rarely observable due to the presence of inherent background scattering, both instrumental and, in the case of neutron scattering, also incoherent. A hollow cylinder also follows q^{-1} scattering but, for increasing wall thickness, an intermediate q^{-2} region may be observable. This is shown in Fig. S2† where the background has been deliberately set to zero to demonstrate the series of oscillations extending to high q. Bot and co-workers used this knowledge to enable possible bounds for tubule wall thickness to be obtained.[11]

The SANS intensity is highly dependent on the hydrogen-to-deuterium ratio of the solvent and it is informative to plot the intensity as a function of solvent deuterium level to enable SLD information for the system components to be extracted. Prior to doing so, it is important to recognise that the scattering contains contributions both from the gelators as well as the solvent; to extract only the gelator scattering, the solvent scattering must be subtracted. 32% w/w of gelator is equivalent to 25.6 volume% of gelator in decane (0% C10D) and 28.4 volume% in deuterated decane (100% C10D). Consequently, the SANS requires subtraction of 74.4% and 71.6% of the C10H or C10D signal respectively. The same process needs to be followed to correct the data for intermediate solvent mixtures that contain both C10H and C10D.

Fig. 2 shows the scattering intensity at the principal peak position at 0.1 $Å^{-1}$ as a function of C10D volume fraction. For a single component system in a solvent, *i.e.* a uniform contrast difference, the scattering intensity would be proportional to the square of the scattering contrast. Thus, in a plot of intensity *versus* solvent SLD, the scattering would be expected to follow a parabola and pass through zero at the contrast match point where the solvent SLD matches that of the component. It is apparent from Fig. 2 that while the scattering follows, as expected, a broadly parabolic shape, it exhibits a broad minimum centred at 17(3)% where the number in brackets in the uncertainty in the fit. For comparison, the neutron SLDs are 0.168×10^{-6} and 0.721×10^{-6} $Å^{-2}$ for β-sitosterol and γ-oryzanol respectively. If these molecules, which are present in equimolar ratio here, were intimately mixed then the structural contribution to the oleogel scattering would be contrast matched at an SLD of 0.445×10^{-6} $Å^{-2}$ corresponding to a solvent mixture containing 13.2% C10D.

The SANS from the gels prepared in C10H and C10D is shown in Fig. 3. It is apparent, at these extreme contrasts, that not only has the primary peak intensity changed but there is also a shift in q. This change is inconsistent with the existence of a tubule of uniform composition since, as the contrast varies, only the peak intensity would be expected to change but not its position. This observation agrees with measurements performed on gels and associated emulsions prepared with sunflower oil/decane solvents, where the latter was either non-deuterated or fully deuterated. While there was essentially no difference in scattering between a 90 : 10 and 80 : 20 sunflower oil to decane solvent mixture, when the decane was deuterated, the primary peak varied in position and shape. Note also that complementary SAXS (Fig. 3) indicates a shift in peak position with contrast with the second peak at higher q and third peak at lower q with respect to the corresponding SANS data from the C10D sample.

This observation provides evidence for a tubule structure that is more complex than a simple hollow cylinder with finite wall thickness; consequently a modification of the original

 This journal is © The Royal Society of Chemistry 2022

Open Access Article. Published on 02 June 2022. Downloaded on 12/6/2025 6:49:25 AM.
This article is licensed under a Creative Commons Attribution 3.0 Unported Licence.

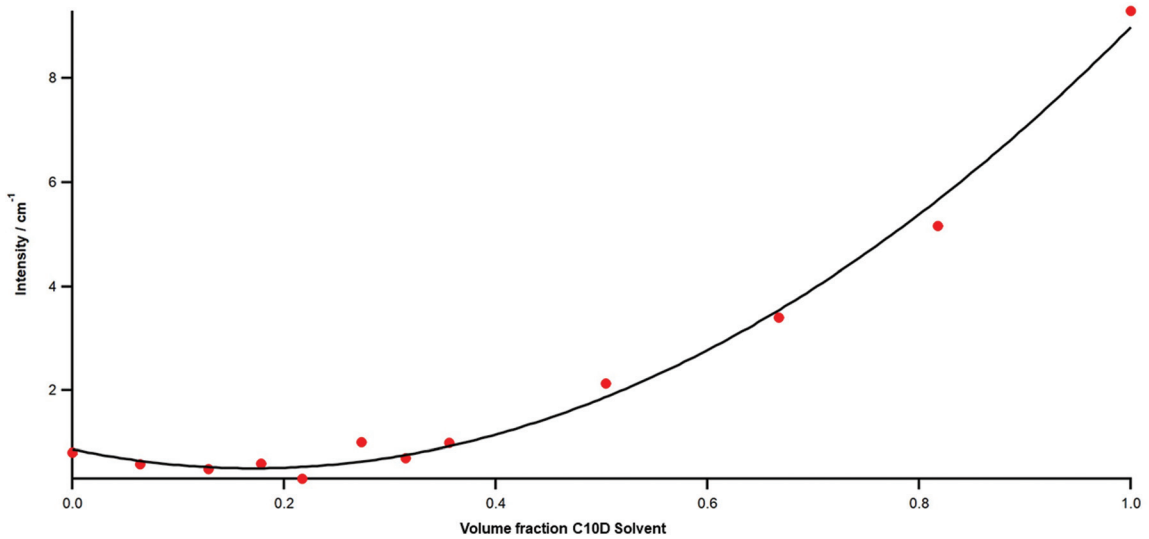

Fig. 2 Integrated intensity at q = 0.1 Å^{-1} as a function of deuterated decane solvent volume fraction in non-deuterated/deuterated solvent mixture following solvent background subtraction.

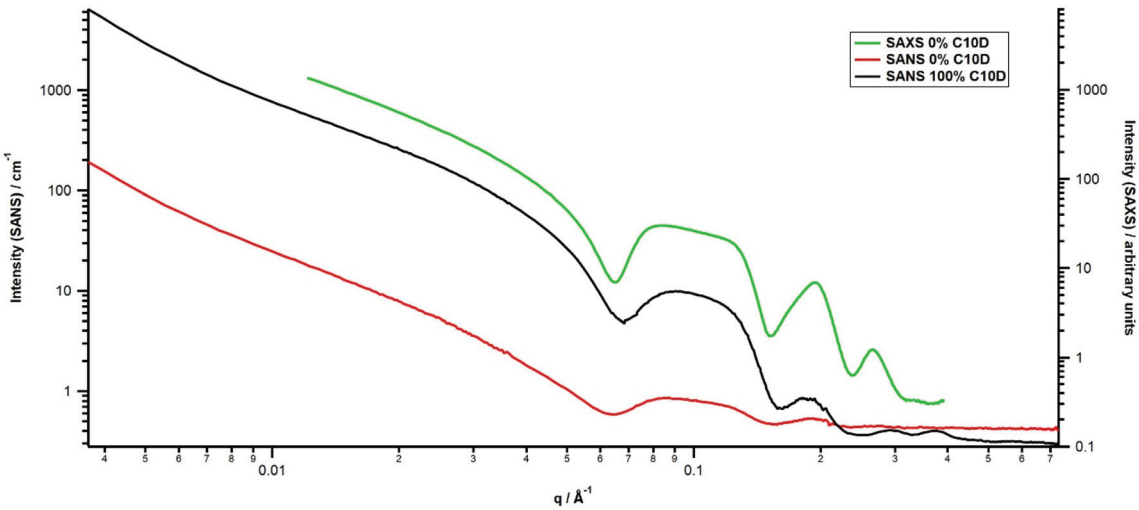

Fig. 3 SANS from gels in non-deuterated and deuterated solvents demonstrating difference in peak shape and position with solvent contrast following solvent background subtraction. SAXS (on arbitrary scale) is also shown for comparison.

model to embrace the concept of a double walled cylinder is justified.[12] The model comprises ten parameters. Four correspond to distances, namely the radius of the core, the inner wall thickness, the outer wall thickness and cylinder length. There are four neutron scattering length densities for the core, inner wall, outer wall and solvent. The last two parameters are scale factor and background. This represents the minimum number of parameters although inevitably one can conceive of additional parameters including size distribution in radius and thickness(es) that could also be included. While this model was formerly employed to fit the gels and associated emulsions, some data sets were excluded due to concern of air being introduced into some of the firm samples thereby affecting the absolute intensity of the SANS, particularly at low q; in addition, bounds for the associated parameters were highly constrained. In the current study, samples have been carefully transferred into demountable cells to minimise air bubbles and a far greater number of multiple contrast samples have been studied. Such an approach provides a rigorous evaluation as to whether a double walled cylinder model is appropriate to describe the tubule structures formed.

While the model comprises a large number of parameters, many can be constrained from knowledge of the formulation. The SLD of each solvent is known and can be fixed. The radius of the core, inner and outer walls can vary but should have the same value independent on contrast. For a hollow cylinder, the core SLD is expected to be the same as the solvent. Since the minimum q of the measurement is much greater than L^{-1},

Open Access Article. Published on 02 June 2022. Downloaded on 12/6/2025 6:49:25 AM.
This article is licensed under a Creative Commons Attribution 3.0 Unported Licence.

the tubule length can be constrained to an arbitrary large value of 6000 Å. Finally, if the data have been collected on an absolute scale, as they are here, the scale factor corresponds to the tubule volume fraction. Global refinement of all twelve scattering patterns can thus be conducted by fixing four parameters and only allowing the radius of the core, the inner and outer wall thicknesses and the inner and outer wall SLDs to vary. However, while acceptable fits could be obtained from individual data sets, significant correlations between fitting parameters were present. More relevant, the model was unsuccessful at describing all the scattering patterns, particularly close to the contrast match point. If one envisages that the inner wall in the cylinder model corresponds to the sterane core and alkyl groups (Table 1 and Fig. S1†) and the outer wall corresponds to the ferulic acid group then, with increasing C10D content, first the inner wall would be contrast matched revealing the outer wall and, at higher C10D content, the opposite. In actuality, no clear demarcation between the molecular regions is apparent; the scattering from the model is far more featured as a function of contrast than that observed experimentally.

Global refinement of all twelve contrasts simultaneously provides further evidence that this model is too simplistic to describe the tubule structure as shown in Fig. 4. A summary of the refined parameters is shown in Table 2. Note that the fitting explicitly considers instrumental resolution effects. The dimensions obtained are physically and chemically sensible, consistent with previous SAXS data, with the neutron SLD values suggesting an outer wall partially solvated by the corresponding solvent (*i.e.* gradual increase in neutron SLD with solvent SLD) while the inner wall SLD of 0.462×10^{-6} Å^{-2} is close to that for androsterol (Table 1). Despite this, it is apparent that the model simply cannot account for the asymmetric primary peak shape. Further evidence for the distorted shape in observed in complementary SAXS (arbitrary intensity) in Fig. 3 as well as higher resolution SANS (through improvements in angular resolution *via* reduced aperture size, and enhanced wavelength resolution by tilting the velocity selector device on QUOKKA; data not shown). This peak shape has been observed in oleogels previously depending on the solvent used. Other scattering functions were considered including double wall elliptical cross-section cylinders and parallelipeds[31] but they were also unable to describe the observed data.

It is known that, at only 5–10% w/w of gelator, organogels can be formed with the mechanical properties approaching those of a block of fat and as low as 2–4% w/w at sub-ambient temperatures.[13] However, the vast majority of studies using SAXS and SANS have used greater concentrations of gelator; indeed, here, 32% w/w gelator has was used. To now, no consideration has been given to the extent to which the individual tubules may interact or the possibility that structure factor effects may therefore be operative. Inevitably some interaction would be expected since the tubules must form a space-filling network for gelling to occur. Unfortunately, while analytical functions, numerical integration and mathematical closure relationships exist to consider a range of structure factor effects to describe the scattering from spherical particles, there are significant challenges to developing similar relationships to describe the scattering from interacting cylinders as a result of the anisometry of the particles. However, an alternative approach is to employ real space modelling which involves constructing scattering units in real space and transforming the model into reciprocal space to reproduce the anticipated scattering.

Fig. 5 shows the scattering following real space reconstruction of an array of extended hollow cylinders arranged such that they aligned parallel to their long axes. While this could also be done for double-walled cylinders, it is sufficient here to

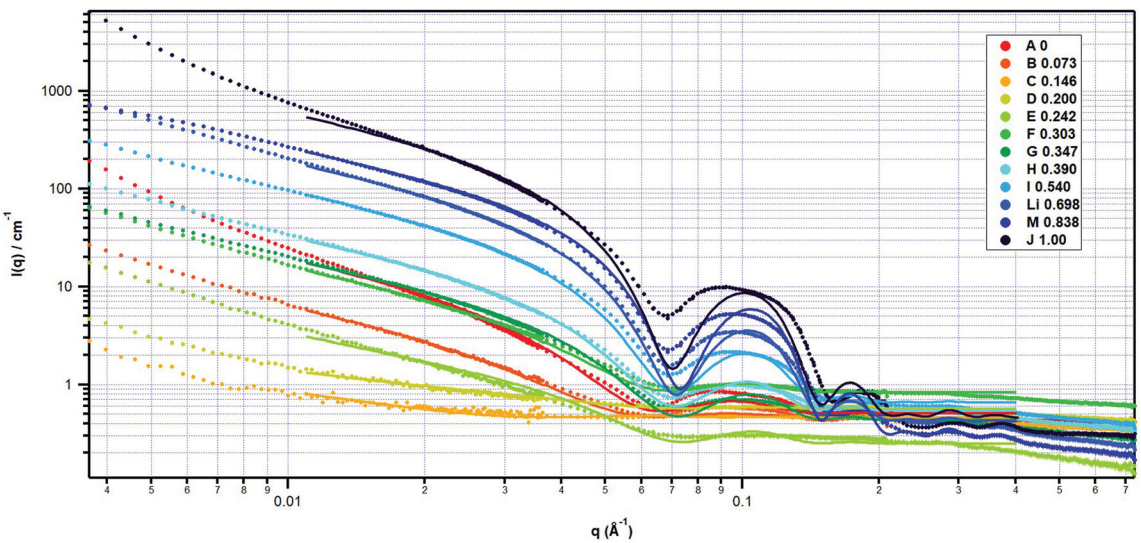

Fig. 4 Global fit to twelve solvent contrast varied data sets, following solvent background subtraction, to double wall cylinder model. Regions exhibiting upturn in scattering at low q as well as high q background have been excluded. Fit parameters are summarised in Table 2.

This journal is © The Royal Society of Chemistry 2022

Open Access Article. Published on 02 June 2022. Downloaded on 12/6/2025 6:49:25 AM.
This article is licensed under a Creative Commons Attribution 3.0 Unported Licence.

Table 2 Fit parameters to globally refined data to double wall cylinder model

Volume fraction C10D	0	0.0642	0.129	0.178	0.217	0.273	0.315	0.356	0.504	0.667	0.818	1.000
Mass fraction C10D	0	0.0734	0.146	0.200	0.242	0.303	0.347	0.390	0.540	0.698	0.838	1.000
sf	0.256	0.258	0.259	0.261	0.262	0.263	0.265	0.266	0.270	0.275	0.279	0.284
r_{core}	22.19(2)											
t_{wall1}	27.81(3)											
t_{wall2}	16.71(6)											
L	6000											
SLD_{core}	−0.488	−0.0345	0.420	0.771	1.05	1.44	1.74	2.03	3.07	4.23	5.29	6.58
SLD_{wall1}	0.462(2)											
SLD_{wall2}	−0.490(4)	1.116(9)	0.230(3)	0.890(2)	1.263(2)	1.598(2)	2.118(3)	2.405(3)	3.662(4)	5.175(6)	6.860(8)	7.72(1)
$SLD_{solvent}$	−0.488	−0.0345	0.420	0.771	1.05	1.44	1.74	2.03	3.07	4.23	5.29	6.58
Background	0.509(2)	0.460(2)	0.461(2)	0.568(2)	0.249(1)	0.839(3)	0.431(2)	0.542(2)	0.654(3)	0.418(2)	0.281(2)	0.455(3)

The number in parentheses corresponds to the uncertainty in the returned value in the fit; however, its value is provided here merely for completeness as the model fails to appropriately describe the scattering data. Values without parentheses have been fixed based on knowledge of the formulation composition. Dimensions are in units of Å; SLD values are in units of 10^{-6} Å^{-2}.

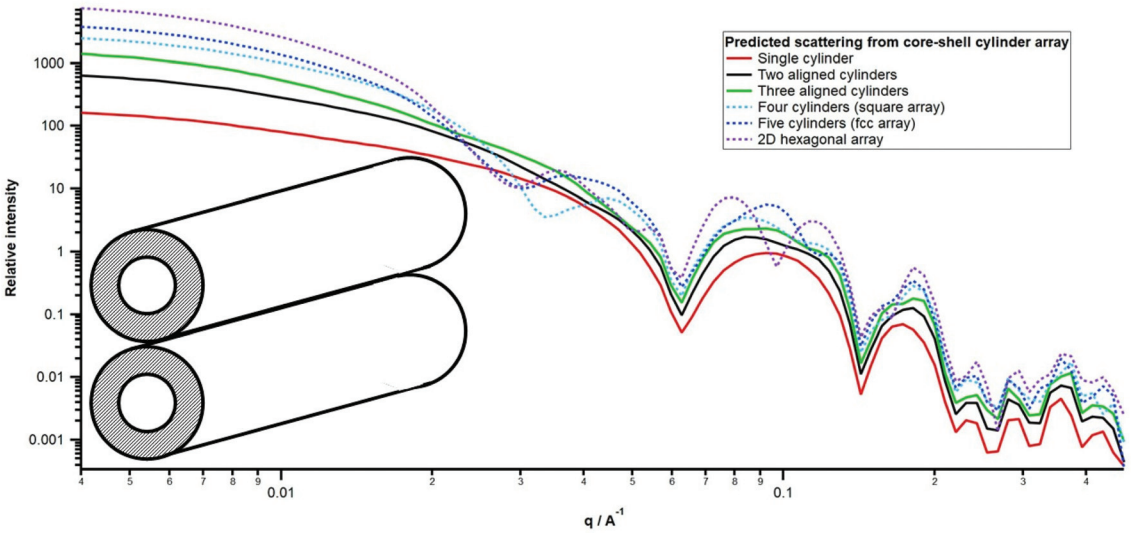

Fig. 5 Real space reconstruction of scattering from array of single wall cylinders (1, 2, 3, 4 in 2D square array, 5 in 2D face centred cubic array and 6 in 2D hexagonal array).

demonstrate the implications to the overall scattering from arrangements of single-walled cylinders. For simplicity, the inner and outer radii have been set as 25 and 50 Å respectively (*i.e.* 100 Å diameter as reported previously) and cylinders have been placed in real space so that they can touch. For the purposes of predicting the shape of the scattering, the actual SLD values are not relevant except that the core and solvent SLDs are equal and different from that of the wall. Data are therefore plotted on a relative intensity scale.

The scattering from a single-walled cylinder is, as expected, consistent with that obtained from its analytical function in reciprocal space. With 2 adjacent cylinders, with a centre-to-centre separation of 100 Å, *i.e.* two hollow cylinders just touching at their outer walls, a distortion of the primary scattering peak is observed that is very similar to that observed here in the SANS and SAXS as well as in previous studies of selected oleogels and associated emulsions. An arrangement of 3 adjacent cylinders in a row results in greater peak distortion. A square array of 4 cylinders, as well 5 in a 2D face centred cubic array and 6 in a 2D hexagonal array, not only result in more extensive splitting of the primary scattering peak but also other peaks at lower q that are not observed experimentally. Interestingly, the arrangement of a limited number of tubules is consistent with atomic force microscopy observations where tubules of approximately 98 Å diameter align to form larger fibrils.[34] Furthermore, such an arrangement is similar to that observed in steroidal systems[22] and has similarities to the gel structures formed by cellulose.[35]

SAXS studies of β-sitosterol : γ-oryzanol gels formed in sunflower oil as a function of concentration (8–100% w/w gelator, *i.e.* the latter being solvent free) also provides supporting evidence. At 8% gelator concentration, the expected range of peaks is observed extending to higher q. However, even at a very high gelator concentration of 95%, these higher angle peaks persist. It is only the primary scattering peak at 0.1 Å^{-1} that becomes increasingly distorted, with major changes

Open Access Article. Published on 02 June 2022. Downloaded on 12/6/2025 6:49:25 AM.
This article is licensed under a Creative Commons Attribution 3.0 Unported Licence.

occurring between 60% and 80% gelator concentration.[17] This is a predictable manifestation of increasing packing density, *via* a structure factor effect, on the overall scattering. It seems likely therefore that such aligned structures are the basis for gelling in these phytosterol-based systems. As an aside, assuming that values for the physical density of the individual components are known, and unchanged on mixing, one may calculate the average centre-to-centre separation, d, between the tubules from knowledge of the mass fraction and therefore volume fraction, vf, and tubule radius, R, *via* the relationship $d = (\pi R^2/\mathrm{vf})^{1/2}$. For example, for 50 Å radius hollow tubules with 25 Å wall thickness in a square array in the C10D solvent (mass fraction = 32%, volume fraction = 28.4%), the centre-to-centre separation would be ≈144 Å. Recent atomistic molecular dynamics simulations have also proposed that the individual tubules can overlap, as opposed to merely touching, to form fibrils.[36] Real space modelling has been conducted to ascertain the scattering from such an arrangement whereby two 50 Å radius tubules have a separation of 80 Å so that the walls of the two tubules overlap by 10 Å. The effect of such overlap is shown in Fig. S3.† As can be seen, no primary peak distortion is observed in the predicted scattering for such a structure although this certainly does not preclude the possibility that such behaviour may occur within this complex system overall.

Conclusions

Contrast variation SANS, as well as SAXS, has been measured on a series of β-sitosterol–γ-oryzanol-based gels formed in non-deuterated/deuterated decane solvents. The primary building blocks of the gels are cylindrical tubules. However, the variation in scattering with solvent contrast cannot be reproduced using a model comprising a single contrast (*e.g.* hollow walled cylinder) as the shape and position of the primary scattering peak changes as a function of solvent contrast. While a more complicated model in which the tubule comprises two walls is able to reproduce peak shifts with varying contrast, it does not describe the scattering well for gels close to their contrast matching condition. This has been rigorously shown from global refinement of twelve individual solvent contrast varied SANS data sets; this illustrates the value of neutron scattering methods combined with the manipulation of contrast to test structural hypotheses. Furthermore, the observed distorted primary scattering peak shape observed here, and previously in other related oleogel and emulsion systems, cannot be reproduced solely with a scattering model based on the form factor from such scattering objects. However, real space modelling suggests that the distorted shape could arise from the assembly of individual tubules to form fibres; the latter is consistent with AFM observations and is likely to be the basis for the gelling mechanism in these systems whereby a connected, space-filling network is generated. One might envisage a system comprising both free tubules and locally aggregated tubules, possibly overlapping, to form fibrils of varying spatial distribution.

It is therefore concluded that the oleogel structure comprises tubules composed of both β-sitosterol–γ-oryzanol that, in turn, form larger scale structures both through intertubule aggregation as well as interconnection *via* junction zones to form a network spanning arrangement. Further experiments with neutron scattering at lower concentrations to limit structure factor effects, even far below that of the concentration at which gelation behaviour occurs, would be valuable to elucidate the structure further. In addition, consideration should be given to use of partially or selectively deuterated structurants that would enable sub-structural details of these gel-forming tubules to be revealed. For example, it may be possible to explicitly investigate the location of alkyl and ferulic acid groups and the extent to which they protrude into the organic solvent. The availability of deuterated triglycerides to better replicate the behaviour of the edible oil phase, as opposed to decane, would also be desirable enabling greater opportunities to exploit contrast variation.

Conflicts of interest

There are no conflicts to declare.

Acknowledgements

The author would like to thank Arjen Bot who first brought this system to his attention in 2009, providing valuable comments to this manuscript and kindly supplying the samples for this study. SANS measurements were performed on QUOKKA as part of proposals P3075 and P1398. The author would also like to thank Marta Martinez-Sanz for assistance with the SAXS measurements. This work benefited from the use of the SasView application, originally developed under NSF Award DMR-0520547. SasView also contains code developed with funding from the EU Horizon 2020 programme under the SINE2020 project Grant No. 654000.

References

1 M. Pernetti, K. F. van Malssen, E. Flöter and A. Bot, *Curr. Opin. Colloid Interface Sci.*, 2007, **12**, 221–231.
2 M. Scharfe and E. Flöter, *Eur. J. Lipid Sci. Technol.*, 2020, **122**, 2000213.
3 J.-M. Lecerf and M. de Lorgeril, *Br. J. Nutr.*, 2011, **106**, 6–14.
4 E. P. Gilbert, in *Fat mimetics for food applications*, ed. M. Cerqueira and L. Castro, John Wiley & Sons (in press).
5 E. P. Gilbert, *Curr. Opin. Colloid Interface Sci.*, 2019, **42**, 55–72.
6 A. Lopez-Rubio and E. P. Gilbert, *Trends Food Sci. Technol.*, 2009, **20**, 576–586.
7 R. d. Adel, P. C. M. Heussen and A. Bot, *J. Phys.: Conf. Ser.*, 2010, **247**, 012025.

 This journal is © The Royal Society of Chemistry 2022

Open Access Article. Published on 02 June 2022. Downloaded on 12/6/2025 6:49:25 AM.
This article is licensed under a Creative Commons Attribution 3.0 Unported Licence.

8 A. Bot and W. G. M. Agterof, *J. Am. Oil Chem. Soc.*, 2006, **83**, 513–521.
9 A. Bot, R. den Adel, C. Regkos, H. Sawalha, P. Venema and E. Flöter, *Food Hydrocolloids*, 2011, **25**, 639–646.
10 A. Bot, R. den Adel and E. C. Roijers, *J. Am. Oil Chem. Soc.*, 2008, **85**, 1127–1134.
11 A. Bot, R. den Adel, E. C. Roijers and C. Regkos, *Food Biophys.*, 2009, **4**, 266–272.
12 A. Bot, E. P. Gilbert, W. G. Bouwman, H. Sawalha, R. den Adel, V. M. Garamus, P. Venema, E. van der Linden and E. Floter, *Faraday Discuss.*, 2012, **158**, 223–238; discussion 239–266.
13 A. Bot, Y. S. J. Veldhuizen, R. den Adel and E. C. Roijers, *Food Hydrocolloids*, 2009, **23**, 1184–1189.
14 M. A. Rogers, A. Bot, R. S. H. Lam, T. Pedersen and T. May, *J. Phys. Chem. A*, 2010, **114**, 8278–8285.
15 H. Sawalha, R. den Adel, P. Venema, A. Bot, E. Floter and E. van der Linden, *J. Agric. Food Chem.*, 2012, **60**, 3462–3470.
16 H. Sawalha, G. Margry, R. den Adel, P. Venema, A. Bot, E. Flöter and E. van der Linden, *Eur. J. Lipid Sci. Technol.*, 2013, **115**, 295–300.
17 H. Sawalha, P. Venema, A. Bot, E. Floter, R. D. Adel and E. van der Linden, *J. Am. Oil Chem. Soc.*, 2015, **92**, 1651–1659.
18 H. Sawalha, P. Venema, A. Bot, E. Flöter, Y. Lan and E. van der Linden, *Food Biophys.*, 2020, **16**, 109–118.
19 H. Sawalha, P. Venema, A. Bot, E. Floter and E. van der Linden, *Food Biophys.*, 2011, **6**, 20–25.
20 F. M. AlHasawi and M. A. Rogers, *J. Am. Oil Chem. Soc.*, 2013, **90**, 1533–1540.
21 S. Calligaris, G. Mirolo, S. Da Pieve, G. Arrighetti and M. C. Nicoli, *Food Biophys.*, 2014, **9**, 69–75.
22 P. Terech and R. H. Wade, *J. Colloid Interface Sci.*, 1988, **125**, 542–551.
23 F. M. Konikoff, D. S. Chung, J. M. Donovan, D. M. Small and M. C. Carey, *J. Clin. Invest.*, 1992, **90**, 1155–1160.
24 P. Terech, A. de Geyer, B. Struth and Y. Talmon, *Adv. Mater.*, 2002, **14**, 495–498.
25 P. Térech, in *Molecular Gels: Materials with Self-Assembled Fibrillar Networks*, ed. R. G. Weiss and P. Terech, Springer Netherlands, Dordrecht, 2006, pp. 275–324, DOI: **10.1007/1-4020-3689-2_11**.
26 S. Cornet, L. de Campo, M. Martínez-Sanz, E. Scholten and E. P. Gilbert, *Innovative Food Sci. Emerging Technol.*, 2021, **73**, 102763.
27 C. V. Nikiforidis, E. P. Gilbert and E. Scholten, *RSC Adv.*, 2015, **5**, 47466–47475.
28 K. Wood, J. P. Mata, C. J. Garvey, C.-M. Wu, W. A. Hamilton, P. Abbeywick, D. Bartlett, F. Bartsch, P. Baxter, N. Booth, W. Brown, J. Christoforidis, D. Clowes, T. d'Adam, F. Darmann, M. Deura, S. Harrison, N. Hauser, G. Horton, D. Federici, F. Franceschini, P. Hanson, E. Imamovic, P. Imperia, M. Jones, S. Kennedy, S. Kim, T. Lam, W. T. Lee, M. Lesha, D. Mannicke, T. Noakes, S. R. Olsen, J. C. Osborn, D. Penny, M. Perry, S. A. Pullen, R. A. Robinson, J. C. Schulz, N. Xiong and E. P. Gilbert, *J. Appl. Crystallogr.*, 2018, **51**, 294–314.
29 S. Kline, *J. Appl. Crystallogr.*, 2006, **39**, 895–900.
30 J. Blazek and E. Gilbert, *Biomacromolecules*, 2010, **11**, 3275–3289.
31 *SASView - Various*, **https://www.sasview.org/**.
32 G. Fritz, *Singlebody*, **https://physchem.kfunigraz.ac.at/sm/Software.htm**.
33 A. H. Larsen, *McSIM*, **https://somo.chem.utk.edu/mcsim/**.
34 A. B. Matheson, G. Dalkas, A. Gromov, S. R. Euston and P. S. Clegg, *Food Funct.*, 2017, **8**, 4547–4554.
35 M. Martínez-Sanz, D. Mikkelsen, B. M. Flanagan, C. Rehm, L. de Campo, M. J. Gidley and E. P. Gilbert, *Polymer*, 2016, **105**, 449–460.
36 G. Dalkas, A. B. Matheson, H. Vass, A. Gromov, G. O. Lloyd, V. Koutsos, P. S. Clegg and S. R. Euston, *Langmuir*, 2018, **34**, 8629–8638.